Structural Engineering and Mechanics, *Vol. 72, No. 5 (2019) 631-642*
DOI: https://doi.org/10.12989/sem.2019.72.5.631

Flexural tests on two-span unbonded post-tensioned lightweight concrete beams

Keun-Hyeok Yang*[1], Kyung-Ho Lee[2a] and Hyun-Sub Yoon[2b]

[1]*Department of Architectural Engineering, Kyonggi University, Suwon, Kyonggi-do, Korea*
[2]*Department of Architectural Engineering, Kyonggi University Graduate School, Seoul, Kyonggi-do, Korea*

(Received July 21, 2018, Revised June 23, 2019, Accepted July 30, 2019)

Abstract. The objective of the present study is to examine the flexural behavior of two-span post-tensioned lightweight aggregate concrete (LWAC) beams using unbonded tendons and the reliability of the design provisions of ACI 318-14 for such beams. The parameters investigated were the effective prestress and loading type, including the symmetrical top one-point, two third-point, and analogous uniform loading systems. The unbonded prestressing three-wire strands were arranged with a harped profile of variable eccentricity. The total length of the beam, measured between both strand anchorages, was 11000 mm. The test results were compared with those compiled from simply supported LWAC one-way members, wherever possible. The ultimate load capacity of the present beam specimens was evaluated by the collapse mechanism of the plasticity theorem and the nominal section moment strength calculated following the provision of the ACI 318-14. The test results showed that the two-span post-tensioned LWAC beams had lower stress increase (Δf_{ps}) in the unbonded tendons than the simply supported LWAC beams with a similar reinforcement index. The effect of the loading type on Δf_{ps} and displacement ductility was less significant for two-span beams than for the comparable simply supported beams. The design equations for Δf_{ps} and Δf_{ps} proposed by ACI 318-14 and Harajli are conservative for the present two-span post-tensioned LWAC beams, although the safety decreases for the two-span beam, compared to the ratios between experiments and predictions obtained from simply supported beams.

Keywords: lightweight concrete, post-tension, two-span beams, load capacity, ductility, ACI 318-14

1. Introduction

Lightweight aggregate concrete (LWAC) has various environmental and structural advantages in terms of lower density and thermal conductivity (Baker 2008, Behnam and Shami 2016). The lower density allows for smaller and lighter weight structural members through the reduction in their self-weight. The smaller and lighter elements are preferred for precast concrete structures because handling and transporting the system becomes less expensive. Meanwhile, there are several structural disadvantages when using LWAC as a building material. The lower modulus of elasticity and tensile resistance capacity of LWAC may cause larger deformations and crack widths in concrete members, undermining the serviceability of structures (Macgregor and Wight 2006). This reduced performance of LWAC members can be compensated by introducing a prestressing force, which is highly effective in minimizing cracks and controlling deflections of flexural members under service loads (Collins and Mitchell 1991). Yang *et al*. (2013a) showed that applying a prestressing force to LWAC flexural members is a quite reliable method for enhancing their serviceability, strength, and ductility.

Reinforced concrete flexural members, including beams and one-way slabs, commonly have several continuous supports. However, the extensive experimental investigations have focused on understanding the flexural behavior of statically-determinate prestressed beams with simple supports. In addition, the derivation and validation of most analytical models for obtaining a rational solution of the stress increase (Δf_{ps}) in the unbonded tendons of post-tensioned flexural members have been based on the idealized plastic region-dependent strain compatibility (Baker 1949, Naaman and Alkhairi 1991) using a bond reduction coefficient and/or an equivalent plastic hinge length (Au and Du 2004, Harajli 2006, Yang *et al*. 2013a) in the simply supported beams. The initial prestress loss and total elongation of unbonded tendons in continuous post-tensioned beams are often measured differently from those of the companion simply supported ones because of the variable friction resistance and concrete strain distribution along the unbonded tendon (Burns *et al*. 1991, Harajli 2012). The spread of the plasticity assumption along the length of member depends on the member continuity and loading pattern. This implies that the increase in strain or stress in the unbonded tendons of post-tensioned continuous beams tends to be diffused by slipping from the yielded to the unyielded span, resulting in lower Δf_{ps} than in simple beams of the same span length, section dimensions, and reinforcement details (Harjli 2012). Hence, the analytical

*Corresponding author, Professor
E-mail: yangkh@kgu.ac.kr
[a] Ph.D. Student
E-mail: horang2@kgu.ac.kr
[b] Ph.D. Student
E-mail: lonsohs@naver.com

ISSN: 1225-4568 (Print), 1598-6217 (Online)

equations for Δf_{ps} derived from the simply supported beams requires further verification and modification for continuous beams.

Several studies (Barbieri *et al*. 2006, Burns *et al*. 1991, Harjli 2012, Lou *et al*. 2016, Moon and Burns 1997, Saeed *et al*. 2015) have examined the overall behavior of two-span post-tensioned beams. However, experimental observations are still needed for evaluating the flexural capacity and Δf_{ps} of post-tensioned beams with different member continuities, loading types, and tendon profiles. Harajli (2012) proposed a parameter that combines the effect of member continuity and type of applied load for calculating Δf_{ps} based on the collapse mechanism of the plasticity theorem. From the general strain compatibility along the equivalent plastic hinge length at the critical sections, he showed that Δf_{ps} is significantly affected by the collapse mechanism and the plastic hinge location of continuous beams. Burns *et al*. (1991) monitored the prestress force in the unbonded tendons of a two-span post-tensioned beam and concluded that the effect of friction losses on the average force in a span should be considered when calculating service load stresses, deflections, and cracking loads. Some researchers (Harajli 2012, Lou *et al*. 2016) revealed the partially contradictory and bad correlated results in post-tensioned continuous beams regarding the safety of the ACI equations (ACI Committee 2014) specified for Δf_{ps}, according to different parameters such as the magnitude of the prestress bar index, member continuity, loading type, concrete compressive strength, and tendon profile. Hence, further studies on experimental and comparative data to examine the reliability of the code specifications need to be conducted for post-tensioned continuous beams. Moreover, the existing knowledge and ongoing investigations on beams using normal-weight concrete (NWC) might be gradually expanded to sustainable elements using LWAC. This is underscored by the growing interest in precast LWAC structures, owing to their various structural and environmental advantages.

The present study tested six two-span LWAC beams post-tensioned using unbonded tendons under symmetrical top one-point, two-point, and analogous uniform loading systems. The incremental stresses (Δf_{ps}) in the unbonded strands measured from the present LWAC specimens were compared with those of the simply supported beams conducted in the previous tests (Yang *et al*. 2013a, b). To evaluate the ultimate loads of beam specimens by the collapse mechanism of the plasticity theorem, the section moment capacities at the sagging and hogging zones of the beam were calculated using the equivalent stress block and stress (f_{ps}) of the unbonded prestressing strands at ultimate member strength, which are specified in the ACI 318-14 provision (ACI Committee 2014). The measured stresses Δf_{ps} and Δf_{ps} were compared with the predicted values by using the design equations proposed by ACI 318-14 and Harajli (2012) in order to examine their potential reliability on two-span post-tensioned LWAC beams.

2. Significance of research

While the ACI 318-14 design procedure for the flexural strength of post-tensioned concrete members has been mostly validated for simply supported NWC beams, the present study provides a novel comparison with the test results obtained from two-span LWAC beams under different loading types. The experimental observations confirm that the effect of loading type on Δf_{ps} and displacement ductility was less significant for two-span beams than for the comparable simply supported beams. This study also ascertained that the ACI 318-14 procedure is conservative for the flexural strength and stresses in the unbonded strands of symmetric two-span post-tensioned LWAC beams, although the safety for Δf_{ps} decreases for two-span beams, compared with the ratios between experiments and predictions obtained from simply supported beams.

3. Experimental program

3.1 Details of specimens

Six symmetric two-span LWAC beams post-tensioned with unbonded strands were prepared for flexural tests, as presented in Table 1. The beam specimens were classified into two groups according to the investigated parameters. The first group was designed to examine the effect of the applied effective prestress (f_{pe}) on the flexural behavior of the post-tensioned beams subjected to two third-point top loads at each span. The magnitude of f_{pe} was varied with 40%, 50%, and 70% of the tensile strength (f_{pu}) of the strands. As for the second group, the beams were under various symmetrical top loading systems at each span, including one-point, two third-point, and analogous uniform loads. The magnitude of f_{pe} in the second group beams was fixed at 60% of f_{pu}. Thus, the specimen notation listed in Table 1 was designated to explain the affiliation of specimen and the parameter investigated in each group. For example, specimen I-0.4 indicates a beam belonging to Group I and subjected to f_{pe} = 0.4 f_{pu}; and specimen II-U refers to a beam under analogous uniform loading in Group II.

All specimens had the same geometrical dimensions and arrangement of their reinforcing bars, as shown in Fig. 1. The width (b_w) and overall depth (h) of the beam section were 205 mm and 350 mm, respectively. The length (L) of a span, measured between the centers of the exterior and intermediate supports, was 5300 mm, and the full length (L_a) of the unbonded tendons, measured between both anchorages, was 11000 mm. Overall, the beam specimens had the same section dimension and one-span length as the previous simply supported beams (Yang *et al*. 2013a). The unbonded tendons were arranged over the full length of the beam with variable eccentricity (harped profile) generating a prestressing moment opposite to the external moment under uniform loads. The eccentricity (e_p) of the harped tendons varied from zero at both exterior supports of the beams to approximately 110 mm at the sagging zone halfway of each span and the hogging zone over the intermediate support. The effective depth (d_s) of conventional non-prestressed longitudinal tensile reinforcement and effective depth (d_p) of the prestressing strands were kept constant to 314 mm and 285 mm,

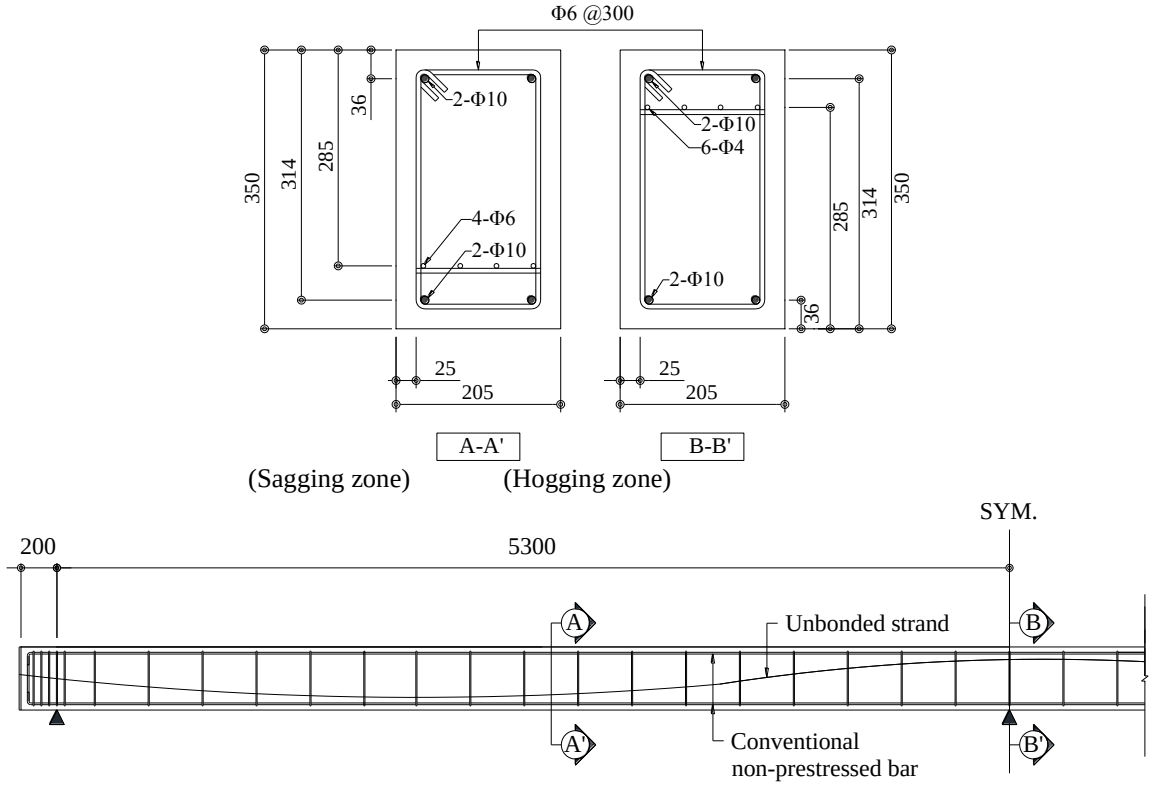

Fig. 1 Details of specimen geometry and arrangement of reinforcement

Table 1 Details of beam specimens

Specimen	$\frac{f_{pe}}{f_{pu}}$	Loading Type	f_c' (MPa)	f_{pe} (MPa)	L (mm)	L_a (mm)	L/d_p	ρ_p	PPR	ω_{pe}
I-0.4	0.4			820						0.0285
I-0.5	0.5	Two-points		1024						0.0356
I-0.7	0.7		39	1434	5300	11000	18.6	0.00137	0.72	0.0499
II-1		One-point								
II-2	0.6	Two-points		1229						0.0428
II-U		Uniform								

respectively, at the sagging and hogging zones for all the beams. As a result, all the beams had L/d_p of 18.6 and L_a/d_p of 38.6.

Four three-wire strands coated with a greased sheath were arranged as post-tensioning tendons. To meet the minimum amount of conventional non-prestressed longitudinal tensile reinforcement specified in ACI 318-14, two deformed bars with a diameter of 10 mm were arranged over the full length of the beam as the top and bottom longitudinal reinforcing bars. Thus, the ratio ρ_p of prestressing strands and partial prestressing ratio $PPR\left(=\frac{A_p f_{pu}}{A_p f_{pu}+A_s f_y}\right)$ of all specimens were approximately constant at 0.0013 and 0.72, respectively, where A_p is the total area of the strands, and A_s and f_y are the total area and yield strength of the conventional non-prestressed longitudinal tensile reinforcement, respectively. The reinforcing index $\omega_{pe}\left(=\frac{A_p f_{pe}+A_s f_y}{b_w d_e f_c'}\right)$ varied within a small range between 0.0285 and 0.0428, as given in Table 1, where d_e is the effective depth of the tensile bars, and f_c' is the compressive strength of concrete. The values of ρ_p, PPR, and ω_{pe} were identical at both the sagging and hogging zones. To prevent anchorage failure of the prestressing strands, closed stirrups with a diameter of 6 mm were arranged at a spacing of 50 mm between the anchorage plate and the exterior supports. For shear reinforcement along the longitudinal axis of the beams, the closed stirrups were arranged at a spacing of 300 mm, which satisfied the minimum requirements specified in the ACI 318-14 shear provision.

3.2 Material properties

Artificially expanded clay granules with maximum sizes

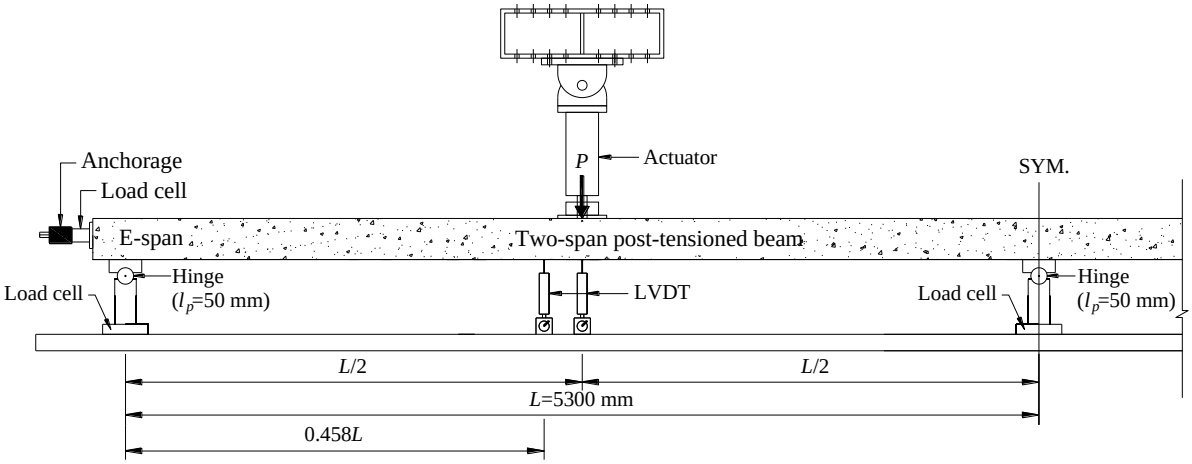

(a) One-point load

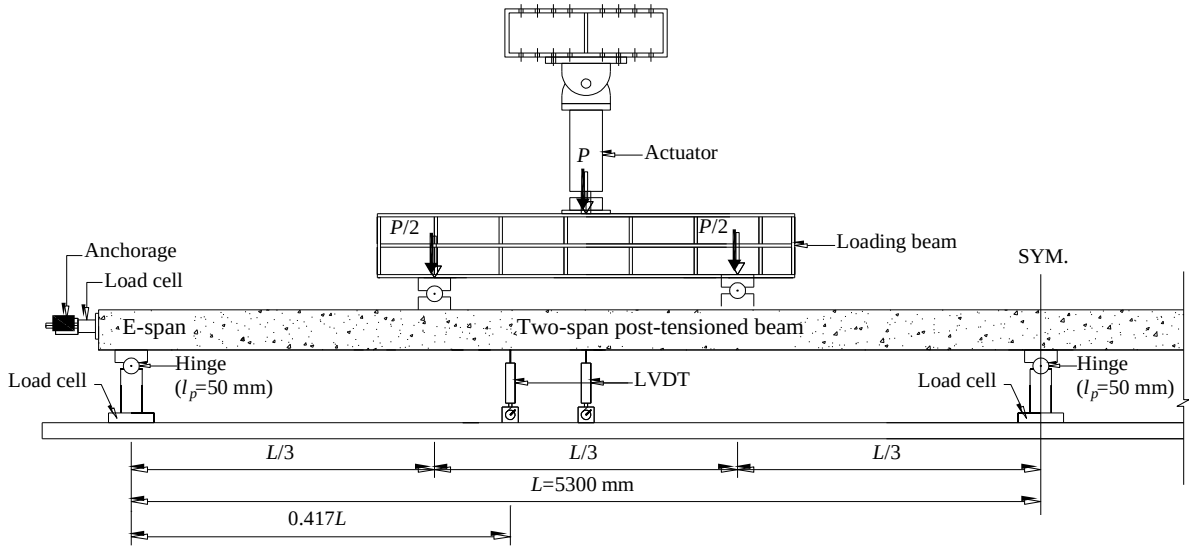

(b) Two third-point loads

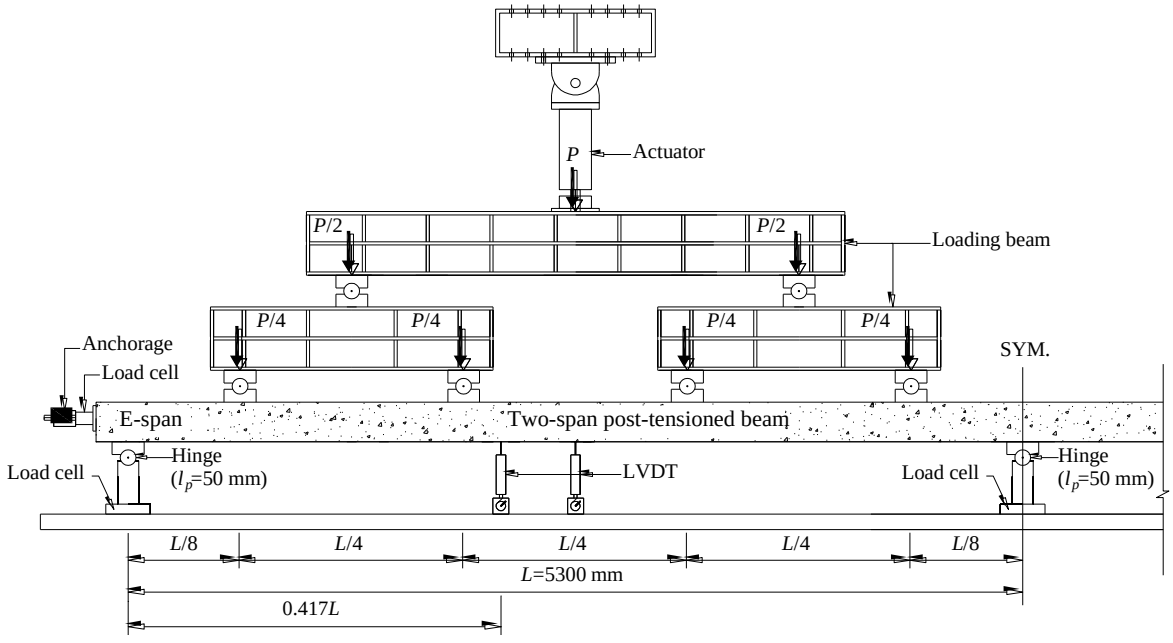

(c) Analogous uniform load

Fig. 2 Test set-up of beams under different loading systems

Table 2 Properties of steel reinforcement

Type	Diameter (mm)	Net Area (mm^2)	Yield Strength (MPa)	Yield Strain	Tensile Strength (MPa)	Elastic Modulus (GPa)
Non-pressed bar	6	28.26	399	0.00386	445	204
	10	71.30	446	0.00217	570	205
3-wire strand	2.9	19.82	1741	0.01	2048	202

of 5 mm and 20 mm were used for lightweight fine and coarse aggregates, respectively, to produce ready-mixed LWAC. The lightweight aggregate featured a spherical shape of closed surface with a slightly rough texture. The core of the particles had a uniformly fine and porous structure. For adequate particle distribution, the lightweight fine aggregates were replaced with local natural sand of maximum size below 2.5 mm by 30% (in volume). The designed density and compressive strength of LWAC were 1750 kg/m^3 and 35 MPa, respectively. Control specimens, cylinders of 150 × 300 mm, were cast and cured simultaneously with the beam specimens in order to determine the average dry density (w_c) and f_c' of the produced LWAC. The measured w_c and f_c' at the time of the beam tests were approximately 1770 kg/m^3 and 39 MPa, respectively.

The mechanical properties of the steel reinforcement used in the specimens are listed in Table 2. The low relaxation three-wire mono-strand with a nominal diameter of 2.9 mm used as prestressing steel did not exhibit a yield plateau. Based on a 1% strain, the yield strength (f_{py}) was determined to be 1741 MPa, which corresponded to 85% of the tensile strength (f_{pu}). The elongation strain at fracture of the strand reached only 5.1%, indicating a low ductile property. The yield strengths of the conventional non-prestressed reinforcing bars with diameters of 6 mm and 10 mm were 399 MPa and 446 MPa, respectively.

3.3 Testing and measurement

Figure 2 shows the different loading systems and instrumentation arrangements prepared for the present beam tests. All beams having two spans were tested to failure under different symmetrical top loading systems with a displacement rate of 2.5 mm/min using a 500 kN capacity actuator at each span. Each span was identified as either E-span or W-span. To simulate a uniform load, top loads were distributed uniformly at four points using steel beams at each span. The two exterior end supports were designed to allow horizontal and rotational movements, whereas the intermediate support prevented horizontal movement but allowed rotation. At the location of the loading or support point, a steel plate with dimension of 50 mm wide and 50 mm thick was provided to prevent premature bearing failure of concrete. At both exterior supports, load cells were installed to measure the shear and reaction distributions. Immediately before the test set-up of each specimen, a designed prestressing force was applied to the unbonded tendons, which were subsequently anchored using a wedge set at both ends of the beam. The stress increase of the unbonded strands according to the applied load was recorded using 100 kN capacity load cells installed between the anchor plate and the wedge set. All beams were preloaded up to a top load of 10 kN at each span before full-scale testing to assure a similar loading distribution to the supports, according to the result of the linear two-dimensional finite element (2-D FE) analysis.

The vertical deflections of each beam were measured using linear variable differential transducers (LVDTs) with a gage length of 300 mm at the mid-span and the location of the maximum deflection at each span, as shown in Fig. 2. According to the deflection curve along the beam length predicted by the linear 2-D FE analysis, the location of the maximum deflection from the exterior support was at 0.458L for the one-point loading, and 0.417 L for the two third-point and analogous uniform loading systems. The strains of the concrete extreme fiber in compression and the conventional non-prestressed longitudinal top and bottom reinforcing bars at the sagging and hogging zones were monitored using electrical resistance strain (ERS) gages. At each load increment, the test data were captured by a data logger and automatically stored.

4. Test results and discussion

4.1 Crack patterns and failure modetails of specimens

Figure 3 plots the crack propagation for the beam specimens at different load levels up to failure. The beams prepared in Group I are not included in the figure because they showed very similar crack patterns and failure modes. This indicates that the propagation rate and the average spacing of the flexural cracks were insignificantly affected by f_{pe}. All the beams showed the crack propagation typically observable at the sagging and hogging zones under flexure, and started to fail with the crushing of the compression concrete at the maximum negative moment region of the hogging zone. Furthermore, diagonal shear cracks within the interior and exterior shear spans and splitting cracks at the anchorage zone of the strands were not developed up to the failure of beams. The above crack performances indicate that the behavior of the beams was governed by flexure. Right before failure, both spans showed the almost same crack patterns. The first flexural crack over the intermediate support generally occurred vertically at about 30–50% of the ultimate strength, indicating that the flexural cracking load tended to increase with the increase in f_{pe}, as presented in Table 3. As the load increased, flexural cracks at the sagging zone appeared, subsequently propagating toward the compression zone. The flexural cracks propagated up to 0.95h at the peak load. The flexural crack zones were mostly concentrated in the maximum moment region at the sagging and hogging zones. The beams of Group II indicate that the flexural crack distribution at the sagging zone was slightly affected by the loading type. The crack zone at the sagging zone was narrower for the beam under one-point top loading than for the beams under two-point and analogous uniform loadings. As a result, the kinking fracture at the sagging zone was more prominent

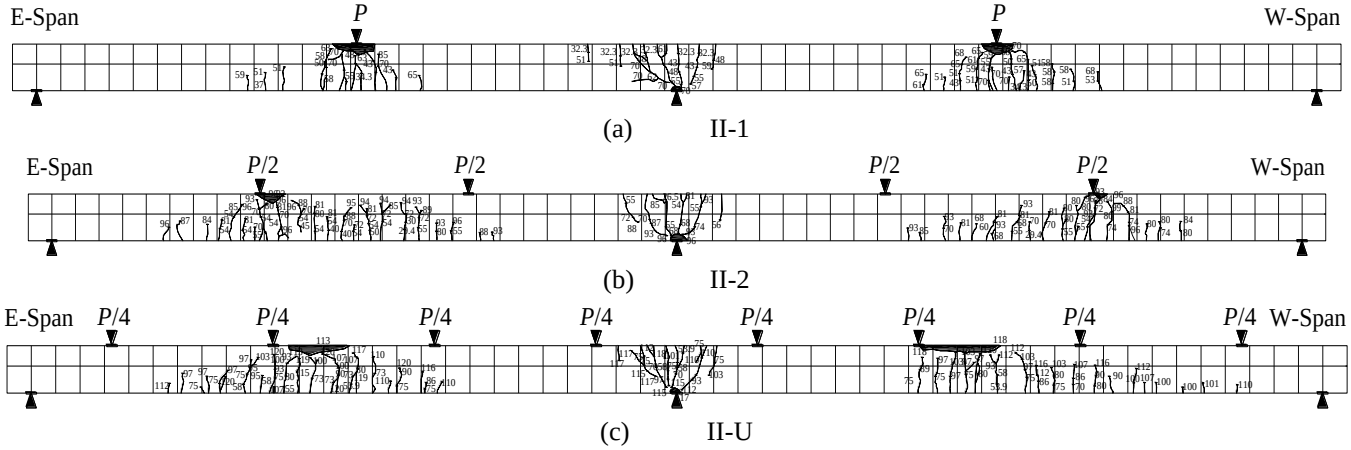

Fig. 3 Crack propagation of the beams in Group II

for the beam under one-point loading than for the beam under two-point loading. Beams II-2 and II-U showed a very similar crack distribution. The crack propagation and distribution at the hogging zone was independent of the loading type. All specimens failed by concrete crushing and buckling of the longitudinal compressive reinforcement at the loading points and at the hogging zone over the intermediated support. The concrete crushing zones were more severe in the beams under one-point and analogous uniform loadings than in the beam under two-point loading.

4.2 Load versus mid-span deflection

The total applied load versus mid-span deflection curves measured at the failed span of the beam specimens are presented in Fig. 4. The beam deflection at mid-span was smaller than that measured at the location of the maximum deflection predicted by the 2-D FE analysis. However, after the yielding of the longitudinal reinforcement at the hogging zone, the mid-span deflection became higher. Thus, the mid-span deflection of each specimen is presented in Fig. 4. All the beams exhibited nearly the same curves at both spans. Before the occurrence of the first flexural crack at the hogging zone, a linear response was observed for all beams. The initial slope slightly increased with the increase in f_{pe} and was slightly higher for the beam under the analogous uniform loading than for the beams under one-point and two-point loading systems. The occurrence of flexural cracks at the hogging and sagging zones caused a decrease in the beam stiffness and an increase in the beam deflection. This stiffness reduction rate was insignificantly affected by f_{pe} and loading type. At the 60−75% peak load, the deflection of the beams increased sharply because of the yielding of the conventional non-prestressed longitudinal tensile reinforcement at the sagging zone. The change of slope at the ascending branch of the curve was more abrupt with the yielding of the conventional non-prestressed tensile reinforcement at the sagging zone than with that at the hogging zone. The response observed after the conventional non-prestressed longitudinal tensile reinforcement yielded can be characterized by a plastic hardening with an extensively increasing rate of deflection under a slow increase in applied load. The plastic hardening response continued up to the first visible crushing of the concrete in compression at the sagging or hogging zone, and thereafter the applied load dropped sharply. The plastic hardening response tended to be shortened with the increase in f_{pe}. Moreover, the beam under one-point loading exhibited a slightly shorter plastic hardening interval than the comparable beams under two-point loading.

4.3 Support reaction

Figure 5 shows the amount of load transferred to the exterior and intermediate supports against the applied load at each span in the beams of Group II. The predictions obtained from the linear 2-D FE analysis are also presented in the same figure. For the applied load (P) at each span, the reactions at the exterior and intermediate supports were calculated at $0.313P$ and $0.687P$, respectively, for one-point load, $0.334P$ and $0.666P$, respectively, for two third-point loads, and $0.372P$ and $0.628P$, respectively, for the analogous uniform loads. The relationship of the exterior and intermediate support reactions against the total applied load were in good agreement with the predictions, regardless of the loading types. This agreement was not affected by the crack occurrence and yielding of the longitudinal reinforcement up to the failure of the beam. This indicates that the internal redistribution of forces is limited in the symmetric two-span post-tensioned beams, although the flexural cracks and yielding of the longitudinal reinforcing bars at the hogging and sagging zones reduce the beam stiffness. However, this limited redistribution would reveal different results for continuous beams with different amount of longitudinal reinforcement at the sagging and hogging zones. Mun and Yang (2018) reported that a slightly lower moment redistribution was obtained for externally post-tensioned beams with a greater amount of longitudinal reinforcement at the sagging zone. In addition, Lou *et al*. (2014) showed that the ratio of longitudinal reinforcement amount between sagging and hoggin zones is one of the most important factors for moment redistribution of post-tensioned beams.

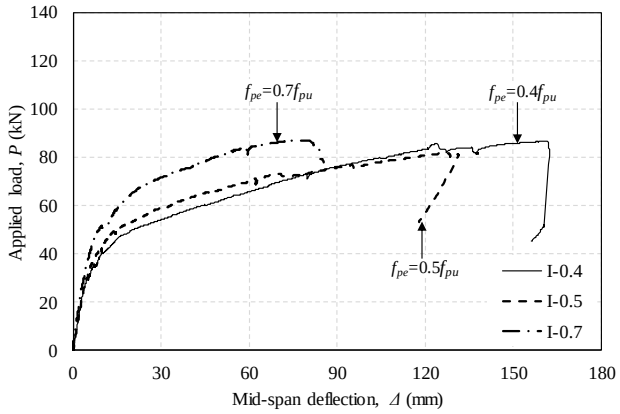

(a) Beams of Group I

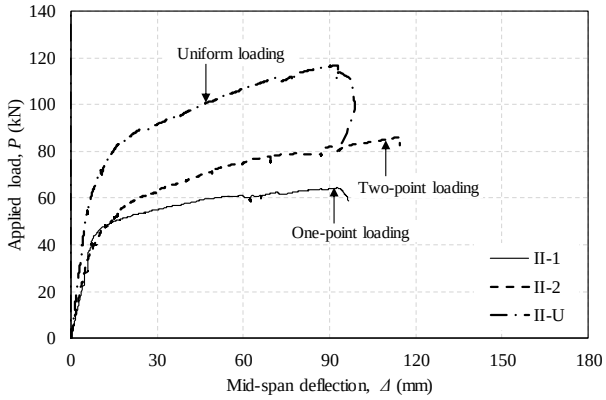

(b) Beams of Group II

Fig. 4 Mid-span deflection against the applied load

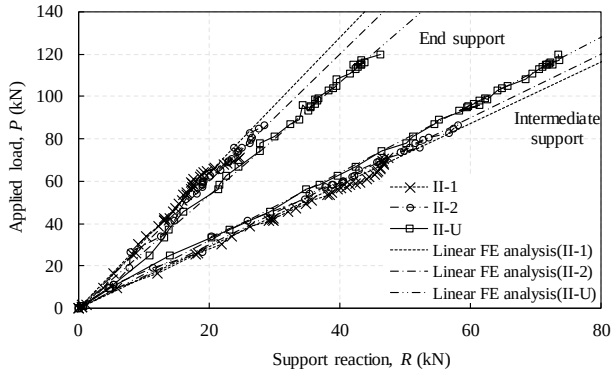

Fig. 5 Support reaction against the applied load

4.4 Stress increase of unbonded prestressing strands

The stress increase of the unbonded prestressing strands in different beams against the applied load at each span is shown in Fig. 6. The stress of the prestressing strands was calculated from the average forces recorded in the load cells installed at both ends of beams. The stress-increase behavior of the prestressing strands measured in the two-span beams was very close to that commonly observed in simply supported beams (Yang *et al*. 2013a). The stress of the prestressing strands was not variable until the occurrence of the first flexural crack at the sagging zone, beyond which the stress increased gradually with the increase in the applied load. The shape and attributes of the load-stress increase curves of the prestressing strands after the occurrence of the flexural crack were very similar to those of the load-deflection curves of the beams, indicating that the stress increase of the unbonded prestressing strands significantly depends on the magnitude of the beam deflection. The increasing rate of the stress was slightly greater in beams with a lower f_{pe}. As a result, a greater value of Δf_{ps} at ultimate state was obtained in beams with a lower f_{pe}, as given in Table 3. In addition, the value of Δf_{ps} was marginally affected by the loading type. It is commonly recognized (Harajli 2006, Naaman and Alkhairi 1991, Yang *et al*. 2013b) that Δf_{ps} in simple beams is commonly higher for two-point or uniform loading systems than for one-point loading, because a greater equivalent plastic hinge length at the sagging zone is formed in the former beams, compared to the latter ones. The present Group II beams revealed that the effect of loading type on Δf_{ps} could be mitigated with the increase in continuity. This may be attributed to the fact that the equivalent plastic hinge length and frictional resistance in the unbonded strands at the hogging zone was nearly independent of the loading type. However, this observation needs to be further verified for different parameters, including L_a/d_p, PPR, ω_{pe}, and loading patterns.

Figure 7 shows the relationship between ω_{pe} and Δf_{ps}, measured in post-tensioned LWAC beams under symmetrical top loads. The simple LWAC beams and one-way slabs tested by Yang *et al*. (2013a, b) were used for the comparisons. The geometrical dimension of the simple beams was the same as the present continuous beams. The LWAC beams potentially have higher Δf_{ps} than the comparable normal-weight concrete (NWC) beams with the same ω_{pe} value because of the lower modulus of elasticity and tensile resistance of this material (Yang *et al*. 2013a). With the increase in ω_{pe}, Δf_{ps} tended to decrease. This is because the reduction of the moment of inertia caused by the crack propagation is less in the beams with a higher ω_{pe} value, which results in a smaller beam deflection. At the same value of ω_{pe}, Δf_{ps} measured in two-span beams was lower than that of the comparable simple beams and one-way slabs. This may be attributed to the fact that the two-span beams generally have smaller total deformation along the beam length and greater frictional loss of stress in the unbonded strands at the hogging zone than the simply supported beams with the same span length (Collins and Mitchell 1991).

4.5 Ultimate load capacities

The collapse loads of two-span beams can be determined based on the principle of virtual work. In general, all deformations of a structure at collapse arise from a rotation at the plastic hinges (Park and Paulay 1975). The plastic hinges in the current beam system can be formed at the maximum moment points at the sagging zone and at the hogging zone over the intermediate support, as shown in Fig. 8. Considering the deflections and rotations as virtual displacements, the ultimate load capacity of the beam can be determined by equating the external virtual work conducted by the applied loads and the internal virtual work absorbed by the hinge rotation. Overall, the following

Table 3 Summary of test results

Specimen	Initial flexural cracking load (kN)		Yielding load (kN)		Ultimate load (P_n) and reactions (R_n) at failed span (kN)			Δ_{cr} (mm)	Δ_y (mm)	Δ_n (mm)	f_{ps} (MPa)	Δf_{ps} (MPa)	$(M_p)_{ACI}$ (kN·m)	$(P_n)_{Pre.}$ (kN)	$\frac{(P_n)_{EXP.}}{(P_n)_{Pre.}}$	μ
	$(P_{cr})_H$	$(P_{cr})_S$	$(P_y)_H$	$(P_y)_S$	P_n	$(R_n)_I$	$(R_n)_E$									
I-0.4	30.4	30.4	38.7	48.9	86.6	56.5	29.3	4.7	10.8	162.2	1859.0	1039.8	44.7	67.5	1.28	15.0
I-0.5	29.4	31.4	45.1	59.5	81.2	53.4	28.0	3.7	11.2	131.1	1792.0	768.0	48.9	73.8	1.10	11.7
I-0.7	51.0	51.0	50.3	63.6	87.0	57.2	30.3	12.2	10.8	80.9	1872.3	438.7	56.2	86.4	1.01	7.5
II-1	32.3	34.3	37.1	42.7	64.3	42.5	21.6	3.6	12.3	92.4	1758.3	529.5	53.1	60.1	1.07	7.5
II-2	26.5	29.4	47.3	58.2	85.2	54.9	30.9	3.1	12.9	111.7	1871.3	642.5	53.1	80.1	1.06	8.7
II-U	53.9	53.9	61.4	85.2	116.7	72.5	43.8	5.0	13.9	95.7	1787.6	558.8	53.1	110.2	1.06	6.9

* Note: The subscripts H and S refer to the hogging and sagging zones, respectively. In addition, the subscripts I and E indicate the intermediate and exterior supports, respectively

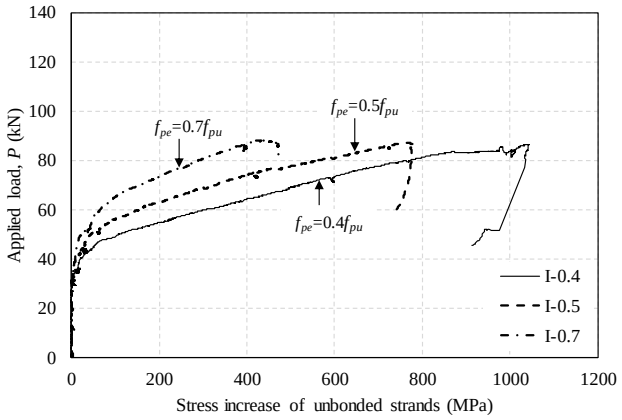

(a) Beams of Group I

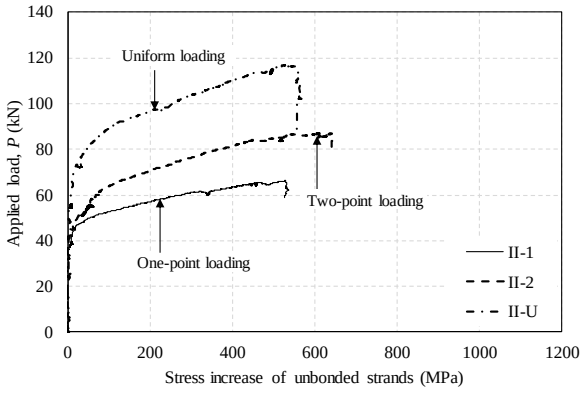

(b) Beams of Group II

Fig. 6 Stress increase in unbonded strands against applied load

relationships for the ultimate load capacity (P_n) at each span of the current beams can be obtained

$$P_n = \frac{4M_p^+ + 2M_p^-}{L} \quad \text{for one-point top loading} \qquad (1.a)$$

$$P_n = \frac{6M_p^+ + 2M_p^-}{L} \quad \text{for two-third top loading} \qquad (1.b)$$

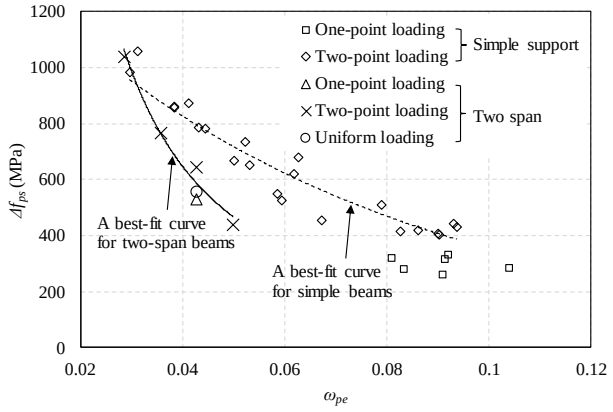

Fig. 7 Effect of ω_{pe} on Δf_{ps}

$$P_n = \frac{8M_p^+ + 3M_p^-}{L} \quad \text{for analogous uniform loading} \qquad (1.c)$$

where M_p^+ and M_p^- are the nominal ultimate moments of the beams at the sagging and hogging zones, respectively. All the beams had the same details for geometrical dimensions and reinforcement arrangement at the sagging and hogging zones. This implies that both of M_p^+ and M_p^- are identical for all the beams. Using the equivalent rectangular compressive stress distribution specified in ACI 318-14 for NWC, the nominal ultimate moment (M_p) for the present beam section can be calculated using the following equation

$$M_p = A_p f_{ps}\left(d_p - \frac{a}{2}\right) + A_s f_y\left(d_s - \frac{a}{2}\right) - A_s' f_s'\left(d_s' - \frac{a}{2}\right) \qquad (2)$$

where, d_s' is the depth of the non-prestressed compressive reinforcement, a is the depth of the equivalent rectangular stress block and f_s' (not exceeding f_y) is a stress of the non-prestressed compressive reinforcement. Table 3 displays the predicted values for P_n and M_p obtained using Eqs. (1) and (2). In the predictions for M_p, the value of f_{ps} was determined using the equations of ACI 318-14. As indicated by Eq. (1), the ultimate load capacity of the beam under

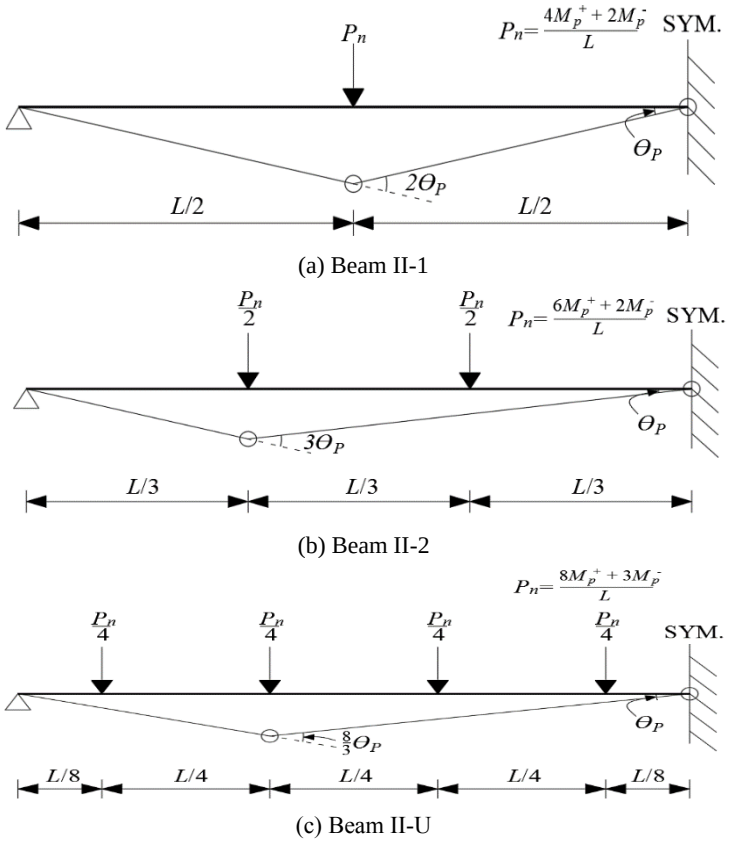

Fig. 8 Collapse mechanism of the present beam systems

analogous uniform load was approximately 1.8 times higher than that of the beam under one-point load. The ratios (γ_p) of the measured and predicted ultimate load capacities tended to decrease with the increase of However, the γ_p values ranged between 1.06 and 1.28 for all the beams. It should be noted that values of γ_p exceeding 1.0 indicate a safe prediction. Hence, M_p and P_n of the two-span post-tensioned beams can be conservatively evaluated using the ACI 318-14 procedure given in Eq. (2) and the collapse mechanism identified in Eq. (1).

4.6 Displacement ductility

The flexural ductility of the tested beams was assessed using a displacement ductility ratio μ ($=\Delta_n/\Delta_y$), where Δ_n and Δ_y are the deflections at the peak load of the beams and at the initial yielding of the longitudinal tensile reinforcement at the hogging zone, respectively. As commonly observed in beams governed by flexure, the displacement ductility decreased with the increase in reinforcing index (or f_{pe}). The value of μ measured in beam I-0.7 was 50% lower than that of beam I-0.4, as presented in Table 3. Furthermore, the ductility was marginally affected by the loading type, indicating a 14% lower value of μ for the beam under one-point load than for the comparable beam under two-point loads. However, the effect of the loading type on μ was less significant for two-span beams, compared to the simply supported beams, which show a decreasing rate of 20−30% (Yang *et al*. 2013a, b) for μ under one-point load.

4.7 Comparisons of Δf_{ps} with design equations

The ACI 318-14 equations for Δf_{ps} are based on a limited number of test results (Mattock *et al*. 1971) conducted under the simply supported condition using NWC beams. The equations are formulated as a function of f_c' and prestressing strand ratio (ρ_p) and do not account for the effect of bonded reinforcement, concrete type, loading type, and member continuity on the stress increase in unbonded tendons (Naaman *et al*. 2002). Yang *et al*. (2011, 2013b) revealed that the ACI 318-14 design equations are quite conservative in predicting Δf_{ps} of NWC and LWAC simple beams, although an unsafe condition was occasionally observed in beams with a reinforcing index between 0.27 and 0.35 under one-point top load. Meanwhile, Harajli (2012) pointed out that the ACI 318-14 equations potentially overestimate Δf_{ps} of continuous post-tensioned beams. Thus, he proposed modifications to the ACI 318-14 equations considering the variable plastic hinge formations according to the member continuity and non-symmetrical loading pattern. Ultimately, the present comparison focuses on examining the reliability of the design equations proposed by the ACI 318-14 provision and Harajli for Δf_{ps} and f_{ps} of post-tensioned LWAC one-way members including simply supported members (Yang *et al*. 2013a, b). In applying the equation of Harajli to this comparison, the following assumptions were considered: the stress reduction factor introduced for conservatism is 1.0, regardless of the member continuity; and the minimum

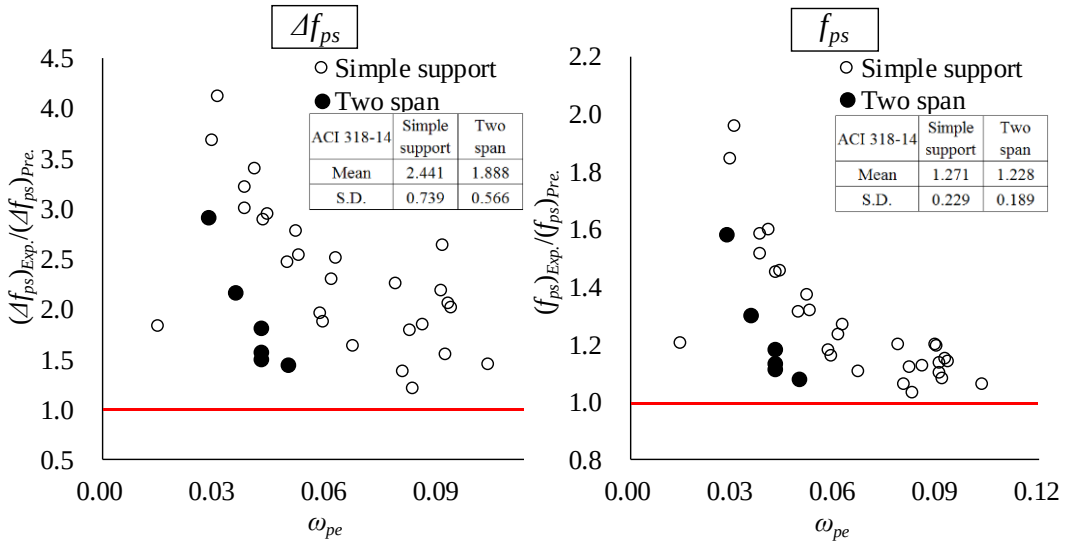

(a) ACI 318-14 equations

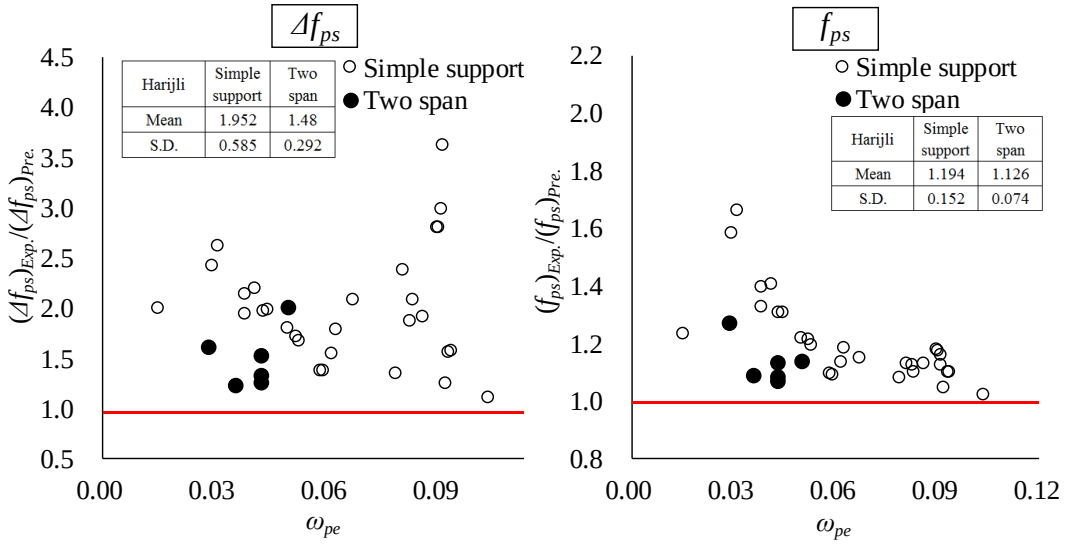

(b) Harajli equations (considering the member continuity)

Fig. 9 Comparison between the measured stresses in the unbonded tendons and predicted values

number of positive and negative plastic hinges is 1.0 and 0.0, respectively, for simply supported members.

Figure 9 plots the ratios of experimental results and predictions for Δf_{ps} and v of the post-tensioned LWAC one-way members. Those comparisons for the present beam specimens are also summarized in Table 4. From the database (Yang *et al*. 2013b) compiled from simply supported post-tensioned NWC beams including 180 datasets, the mean and standard deviation of the ratios determined using the ACI 318-14 equations were 1.949 and 0.773, respectively, for Δf_{ps}, and 0.988 and 0.419, respectively, for f_{ps}. For the post-tensioned simply supported LWAC members, the mean and standard deviation were 2.441 and 0.739, respectively, for Δf_{ps}, and 1.271 and 0.229, respectively, for f_{ps}, as shown in Fig. 9 (a). For the two-span post-tensioned LWAC members, the mean and standard deviation were 1.888 and 0.566, respectively, for Δf_{ps}, and 1.228 and 0.189, respectively, for f_{ps}. This indicates that the ACI 318-14 equations are still conservative for the present two-span post-tensioned LWAC beams, and the safety decreases for two-span beams, compared with the ratios between experiments and predictions obtained from the simply supported beams.

The equations proposed by Harajli are also conservative for the LWAC beams. The mean and standard deviation of the ratios determined using datasets for the simply supported LWAC members are 1.952 and 0.585, respectively, for Δf_{ps}, and 1.194 and 0.152, respectively, for f_{ps}, as depicted in Fig. 9 (b). Those values obtained for the present two-span LWAC beams are 1.480 and 0.292, respectively, for Δf_{ps}, and 1.126 and 0.074, respectively, for f_{ps}. This indicates that the predicted values obtained from the Harajli equations are in good agreement with the test results of the present two-span LWAC beams, although the safety level tends to decrease for two-span LWAC beams, compared with the trend observed in simply supported LWAC beams.

Although a conservative evaluation is obtained to apply the design equations of Δf_{ps} and f_{ps} for the two-span post-tensioned LWAC beams, the ratios of experiments and

Table 4 Comparisons of the measured Δf_{ps} and f_{ps} with the predicted values

Specimens	Experiments		Predicted values by design equations				Exp./Pre.			
			ACI 318-14		Harajli		ACI 318-14		Harajli	
	f_{ps} (MPa)	Δf_{ps} (MPa)	f_{ps} (MPa)	Δf_{ps} (MPa)	f_{ps} (MPa)	Δf_{ps} (MPa)	f_{ps}	Δf_{ps}	f_{ps}	Δf_{ps}
I-0.4	1859.0	1039.8	1176.6	357.4	1469.4	650.2	1.58	2.91	1.27	1.60
I-0.5	1792.0	768.0	1381.4	357.4	1654.0	630.0	1.30	2.15	1.08	1.22
I-0.7	1872.3	438.7	1741.0	307.4	1654.0	220.4	1.08	1.43	1.13	1.99
II-1	1758.3	529.5	1586.2	357.4	1654.0	425.2	1.11	1.48	1.06	1.25
II-2	1871.3	642.5	1586.2	357.4	1654.0	425.2	1.18	1.80	1.13	1.51
II-U	1787.6	558.8	1586.2	357.4	1654.0	425.2	1.13	1.56	1.08	1.31

predictions tend to decrease with the increase in ω_{pe}, showing a more noticeable drift for the ACI 318-14 equations. Hence, the reliability of the design equations needs to be further examined for beams with higher ω_{pe} and increased member continuity.

5. Conclusions

The present study examined the flexural behavior of two-span unbonded post-tensioned LWAC beams under different loading types. The test results were compared with those of the simple LWAC beams compiled from the previous investigations, wherever possible. The incremental stress (Δf_{ps}) and ultimate stress (f_{ps}) in the unbonded strands measured at the peak state of the beams were compared with the design equations proposed by the ACI 318-14 provision and Harajli, considering the member continuity. From the experimental observations and comparisons to ascertain the reliability of the design equations for two-span LWAC beams, the following conclusions were drawn:

- The flexural crack zone at the sagging zone was narrower for the beam under one-point top loading than for the beams under two-point and analogous uniform loadings, whereas the crack propagation and distribution at the hogging zone was independent of the loading type.
- The reactions measured at each support were consistent with the predictions calculated from a linear two-dimensional finite element analysis, indicating that the internal redistribution of forces is limited in the symmetrical two-span post-tensioned beams although flexural cracks and yielding of the longitudinal reinforcing bars at the hogging and sagging zones reduce the beam stiffness.
- The effect of loading type on Δf_{ps} was less significant for the two-span beams than for the comparable simply supported beams.
- At the same value of reinforcement index (ω_{pe}), Δf_{ps} measured in the two-span beams was lower than that in the simple beams and one-way slabs.
- The displacement ductility ratio (μ) was 14% lower for the beam under one-point load than for the comparable beam under two-point loads, indicating that the effect of loading type on μ was less significant for two-span beams than for the simply supported beams.
- The ultimate load capacity (P_n) of the two-span post-tensioned LWAC beams can be conservatively evaluated using the ACI 318-14 procedure including an equivalent rectangular stress block and the collapse mechanism of the plasticity theorem.
- The design equations for Δf_{ps} and f_{ps} proposed by ACI 318-14 and Harajli are conservative for the present two-span post-tensioned LWAC beams, although the safety decreases for two-span beams, compared to the ratios between experiments and predictions obtained from the simply supported beams.

Acknowledgments

This work was supported by the National Research Foundation of Korea (NRF) grant funded by the Korea Government (MSIP) (No. NRF-2017R1A2B3008463) and Basic Science Research Program through NRF funded by the Ministry of Science, ICT & Future Planning (No. 2015R1A5A1037548).

References

Au, F.T.K. and Du, J.S. (2004), "Prediction of ultimate stress in unbonded prestressed tendons", *Mag. Concrete. Res.*, **56**(1), 1-11.

Baker, A.L.L. (1949), "A plastic theory of design for ordinary reinforced and prestressed concrete including moment redistribution in continuous members", *Mag. Concrete. Res.*, **1**(2), 57-66.

Baker, O. (2008), "Fly ash lightweight aggregates in high performance concrete", *Constr. Build. Mater.*, **22**(12), 2393-2399. https://doi.org/10.1016/j.conbuildmat.2007.09.001.

Barbieri, R.A., Gastal, F.P.S.L. and Filho, A.C. (2006), "Numerical model for the analysis of unbonded prestressed members", *ASCE. J. Struct. Eng.*, **132**(1), 34-42. https://doi.org/10.1061/(ASCE)0733-9445(2006)132:1(34).

Behnam, V. and Shami, N. (2016), "Self-compacting light-weight concrete; mix design and proportions", *Struct. Eng. Mech.*, **58**(1), 143-161. https://doi.org/10.12989/sem.2016.58.1.143.

Burns, N.H., Helwig, T. and Tsujimoto, T. (1991), "Effective prestress force in continuous post-tensioned beams with unbonded tendons", *ACI. Struct. J.*, **88**(1), 84-90.

Collins, M.P. and Mitchell, D. (1991), *Prestressed concrete structures*, Prentice-Hall, Upper Saddle River, NJ, USA.

Harajli, M.H. (2006), "On the stress in unbonded tendons at ultimate: critical assessment and proposed changes", *ACI. Struct. J.*, **103**(6), 1-10.

Harajli, M.H. (2012), "Tendon stress at ultimate in continuous unbonded post-tensioned members: proposed modification of ACI 318, Eq. (18–4) and (18–5)", *ACI. Struct. J.*, **109**(2), 183-192.

Lou, T., Lopes, S.M.R. and Lopes, A.V. (2014), "Factors affecting moment redistribution at ultimate in continuous beams prestressed with external CFRP tendons", *Compos. Part B: Eng.*, **66**, 136-146. https://doi.org/10.1016/j.compositesb.2014.05.007.

Lou, T., Lopes, S.M.R. and Lopes, A.V. (2016), "Response of continuous concrete beams internally prestressed with unbonded FRP and steel tendons", *Compos. Struct.*, **154**, 92-105. https://doi.org/10.1016/j.compstruct.2016.07.028.

Macgregor, J.G. and Wight, J.K. (2006), *Reinforced concrete: mechanics and design*, Pearson Education Limited, London, United Kingdom.

Mattock, A.H., Yamazaki, J., and Kattula, B.T. (1971), "Comparative study of prestressed concrete beams with and without bond", *ACI. J. Proc.*, **68**(2), 116-125.

Moon, J.H. and Burns, N.H. (1997), "Flexural behavior of member with unbonded tendons. I: theory", *ASCE. J. Struct. Eng.*, **123**(8), 1087-1094. https://doi.org/10.1061/(ASCE)0733-9445(1997)123:8(1087).

Mun, J.H. and Yang, K.H. (2018), "Flexural behavior of externally post-tensioned two-span lightweight concrete beams", *Magaz. Concrete. Res.*, https://doi.org/10.1680/jmacr.17.00533.

Naaman, A.E. and Alkhairi, F.M. (1991), "Stress at ultimate in unbonded post-tensioning tendons: part 2-proposed methodology", *ACI. Struct. J.*, **88**(6), 683-692.

Naaman, A.E., Burns, N., French, C., Gamble, W.L. and Mattock, A.H. (2002), "Stresses in unbonded prestressing tendons at ultimate: recommendation", *ACI. Struct. J.*, **99**(4), 518-529.

Park, R. and Paulay, T. (1975), *Reinforced concrete structures*, John Wiley and Sons, New York, NY, USA.

Saeed, G., Ali, A.M., Habib, A.B. and Hamid, R.R. (2015), "Flexural strengthening of continuous unbonded post-tensioned concrete beams with end-anchored CFRP laminates", *Struct. Eng. Mech.*, **53**(6), 1083-1104. http://doi.org/10.12989/sem.2015.53.6.1083.

Yang, K.H. and Kang, T.H.K. (2011), "Equivalent-strain distribution factor for unbonded tendon stress at ultimate", *ACI. Struct. J.*, **105**(2), 217-226.

Yang, K.H. and Mun, J.H. (2013a), "Flexural capacity and stress in unbonded tendons of post-tensioned lightweight concrete beams", *Adv. Struct. Eng.*, **16**(7), 1297-1310. https://doi.org/10.1260/1369-4332.16.7.1297.

Yang, K.H., Mun, J.H. and Kim, G.H. (2013b), "Flexural behavior of post-tensioned normal-strength lightweight concrete one-way slabs", *Eng. Struct.*, **56**, 1295-1307. https://doi.org/10.1016/j.engstruct.2013.07.004.

Yang, K.H., Mun, J.H. and Lee, J.S. (2014), "Flexural tests on pre-tensioned lightweight concrete beams", *P. I. CIVIL. ENG-STR. B.*, **167**(4), 203-216. https://doi.org/10.1680/stbu.12.00003.

CC